applied optics

Quantitative measurement of dynamic nanostrain based on a phase-sensitive optical time domain reflectometer

Yongkang Dong,[1,*] Xi Chen,[1] Erhu Liu,[1] Cheng Fu,[1] Hongying Zhang,[2,3] and Zhiwei Lu[1,4]

[1]National Key Laboratory of Science and Technology on Tunable Lasers, Harbin Institute of Technology, Harbin 150001, China
[2]Institute of Photonics and Optical Fiber Technology, Harbin University of Science and Technology, Harbin 150080, China
[3]e-mail: zhy_hit@163.com
[4]e-mail: lvzw@hit.edu.cn
*Corresponding author: aldendong@gmail.com

Received 26 July 2016; accepted 25 August 2016; posted 29 August 2016 (Doc. ID 270684); published 22 September 2016

A sensing system is proposed for quantitative measurement of large-range dynamic nanostrain based on a phase-sensitive optical time domain reflectometer, where the coherent detection and I/Q demodulation methods are employed to demodulate both the phase and the amplitude of the Rayleigh scattering light in real time. A nanopositioning translation stage is utilized to apply precise nanostrain to fiber. By measuring phase differences between two adjacent sections, the quantitative nanostrain with a large measurement range is demonstrated; this is also a method to measure the strain parameter of refractive index. For the Panda polarization-maintaining fiber under test in the experiment, the strain parameter of phase difference is measured to be 8.714 mrad/(nϵ · m), while the strain parameter of refractive index is measured to be $-0.3751\epsilon^{-1}$. As a proof of the concept, the dynamic strain sensing with a range of 10–1000 nϵ is experimentally demonstrated, and the strain resolution is 1 or 2 nϵ, corresponding to 5 or 2.5 m spatial resolution, respectively. The experimental measurement also shows a triangular wave with a 12-Hz vibrating frequency and a 100-nϵ strain amplitude as well as a 188-Hz resonant signal of the tensile section.

OCIS codes: (060.2310) Fiber optics; (290.5870) Scattering, Rayleigh; (120.4825) Optical time domain reflectometry.

http://dx.doi.org/10.1364/AO.55.007810

1. INTRODUCTION

Strain is an important parameter in the health monitoring of civil structures such as bridges, pipelines, and buildings. To monitor the structural health, various fiber sensors have been researched and developed, such as Brillouin optical time domain analysis (BOTDA), fiber Bragg gratings, and optical frequency domain reflectometers (OFDRs) [1–3]. However, their sensitivity of strain measurement is normally on the order of με, which makes it hard to satisfy the demands of special circumstances, such as crustal deformation measurement [4].

Recently, the phase-sensitive optical time domain reflectometer (Φ-OTDR) has attracted considerable interest due to its highly sensitivity to external perturbations. The principle of Φ-OTDR is based on interference between Rayleigh scattering light from different scattering centers along the fiber within a pulse width [5]. The relative phase change of Rayleigh scattering light is highly sensitive to external perturbations such as vibration, temperature, and strain, which can change the length of the sensing fiber and the effective refractive index at a certain position. A localized phase change can be induced by this, which can finally result in a change of Rayleigh scattering time domain traces. Therefore, a peak appears in the difference trace when subtracting the Φ-OTDR trace from a stable-state one where the position of the peak is the very location of the external perturbation. Several techniques have recently been researched to improve the performance of intrusion detection systems. All-polarization-maintaining configurations of Φ-OTDR were presented for vibration sensing to mitigate polarization-induced signal fading and noise and improve the spatial resolution [6]. Zhu *et al.* demonstrated a vibration sensing system merging a Mach–Zehnder interferometer and Φ-OTDR, of which the maximum frequency response can reach 3 MHz [7], and the authors also used a two-dimensional edge detection method to enhance the signal-to-noise ratio (SNR) and spatial resolution of Φ-OTDR [8]. Wang *et al.* proposed to extend the sensing range to 175 km by using the combination of Raman amplification and Brillouin amplification [9]. However, due to the randomness of the coherent superposition for the Rayleigh scattering light, it is hard to find the quantitative relations between external perturbation and the change of the Rayleigh

scattering time domain trace [10]. Therefore, Φ-OTDR has difficulty measuring strain and temperature quantitatively, so that it is generally utilized as an intrusion detection method.

In essence, the phase change is the most direct reflection of external perturbations. In order to achieve quantitative measurement, it is necessary to research the phase change in detail. Wang *et al.* presented a vibration sensing system based on phase extraction from time-gated digital OFDR to achieve quantitative vibration measurement [11]. Tu *et al.* demodulated phase by utilizing heterodyne detection and I/Q demodulation based on vector BOTDA [12]. In recent years, some research groups have also proposed some methods to research the phase change in Φ-OTDR. Koyamada *et al.* first proposed to measure the strain and temperature by comparing the time domain trace change of Φ-OTDR with a resolution of 0.01°C [13], and they demonstrated it in experiment by shifting the laser frequency to compensate the phase change due to the change of strain and temperature [14]. Because of the process of sweeping frequency, it costs a lot of time during one measurement, which limits this method to be applied to the measurement of static strain. In order to break this limitation, several techniques have been proposed, such as using 3×3 coupler demodulation [15,16], phase generated carrier algorithm [17], digital coherent detection [18], and I/Q demodulation and homodyne detection [19]. Tu *et al.* developed the Φ-OTDR system for quantitative vibration measurement for the first time, but the range and precision of measurement remain to be improved [20]. All of those methods get a good result of phase demodulation and achieve dynamic strain sensing. However, they usually used piezoelectric ceramic transducer (PZT) to apply strain, and the precision of measurement was restricted; thus the relation between phase difference and strain has no precise quantitative research, and the range of measured strain is too small.

In this paper, we demonstrate the quantitative measurement of nanostrain distributed sensing with a large strain measurement range based on Φ-OTDR by utilizing coherent detection and I/Q demodulation. Both the phase and the amplitude of the Rayleigh scattering light can be demodulated in real time. The nanopositioning translation stage is utilized to apply nanostrain to fiber, which can supply more precise strain than PZT. The phase difference between two adjacent sections is utilized to measure nanostrain quantitatively, and the strain sensitivity of our system is measured to be 8.714 mrad/(nϵ · m), while the strain parameter of refractive index C_ϵ is measured to be $-0.3751\epsilon^{-1}$. The experimental setup and measurement principle are illustrated in subsequent sections, and the performance of our sensing system is experimentally demonstrated.

2. PRINCIPLE

In the Φ-OTDR system, light pulses with narrow linewidth are injected into the sensing fiber, and the Rayleigh backscattering light reflected from numbers of scattering centers forms the signal light, which is a plot of optical power versus time. The coherent detection can be seen as the signal light beat with the local light. The signal and local light can be expressed as [21]

$$E_S(t) = A_S(t)\cos\theta_S \exp j[2\pi(\nu+\Delta f)t+\varphi(t)+\varphi_1], \quad (1)$$

$$E_{\mathrm{LO}}(t) = A_{\mathrm{LO}}\cos\theta_{\mathrm{LO}} \exp j(2\pi\nu t+\varphi_2), \quad (2)$$

where $A_S(t)$ and A_{LO} are the amplitude of the signal light and local light, θ_S and θ_{LO} represent the polarization direction, ν is the frequency of quasi-monochromatic light, and Δf is the frequency shift of the signal light, which is usually generated by an acousto-optic modulator (AOM). $\varphi(t)$ is the phase change terms of signal light, and φ_1 and φ_2 are the initial phase of the signal light and local light, respectively. The Rayleigh backscattered signal light will be mixed with the local light by a 3 dB coupler. Then the mixed signal is launched to a balanced detector, and the AC component can be obtained by using heterodyne detection. The detected current is proportional to the optical power,

$$I(t) \propto 2A_S(t)A_{\mathrm{LO}}\cos\theta_S\cos\theta_{\mathrm{LO}} \times \cos[2\pi\Delta f t+\varphi(t)+\varphi_1-\varphi_2]. \quad (3)$$

From Eq. (3), we can see that the detected current contains the phase and the amplitude of the Rayleigh scattering light, and we can control the local light power to enhance the detected current. Besides, for the purpose of obtaining the most powerful signal, it is necessary to ensure that the signal light and local light have the same polarization direction. The detected current can be rewritten as $I_S(t)\cos[2\pi\Delta f t+\varphi(t)]$, and essentially it is a signal with phase modulation and amplitude modulation. Then we demodulate the phase $\varphi(t)$ and the amplitude $I_S(t)$ by using I/Q demodulation.

Figure 1 shows the fundamental principles of I/Q demodulation [12,19]. The heterodyne signal we detected is $I_S(t)\cos[2\pi\Delta f t+\varphi(t)]$, and the local signal can be described as $I_{\mathrm{LO}}\sin(2\pi\Delta f t)$, where I_{LO} is the amplitude of the local signal. Before mixing with the heterodyne signal, the local signal should be split into two parts; one part is applied with $\pi/2$ phase shift, and another one keeps the initial phase. Then the two outputs of the hybrid can be obtained as

$$I_S(t)I_{\mathrm{LO}}\cos[2\pi\Delta f t+\varphi(t)]\sin(2\pi\Delta f t), \quad (4)$$

$$I_S(t)I_{\mathrm{LO}}\cos[2\pi\Delta f t+\varphi(t)]\sin(2\pi\Delta f t+\pi/2). \quad (5)$$

According to the product to sum formula, we can get

$$\frac{1}{2}I_S(t)I_{\mathrm{LO}}\{\sin[4\pi\Delta f t+\varphi(t)]-\sin[\varphi(t)]\}, \quad (6)$$

$$\frac{1}{2}I_S(t)I_{\mathrm{LO}}\{\cos[4\pi\Delta f t+\varphi(t)]+\cos[\varphi(t)]\}. \quad (7)$$

Each of the two outputs of the hybrid is then low pass filtered to remove the high frequency component by low pass filters (LPFs), generating the in-phase component $I(t)$ and quadrature component $Q(t)$, which can be expressed as

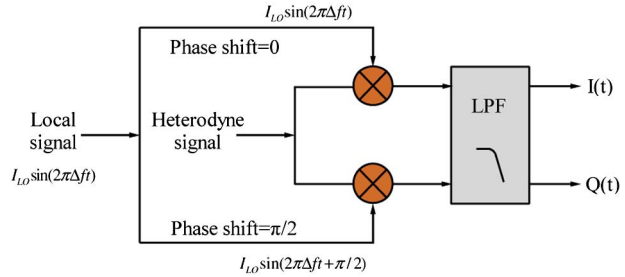

Fig. 1. I/Q demodulation schematic diagram.

$$I(t) = \frac{1}{2} I_S(t) I_{\mathrm{LO}} \sin[\varphi(t)], \tag{8}$$

$$Q(t) = \frac{1}{2} I_S(t) I_{\mathrm{LO}} \cos[\varphi(t)]. \tag{9}$$

Then the amplitude and phase of the Rayleigh scattering light can be expressed as

$$I_S \propto \sqrt{I^2(t) + Q^2(t)}, \tag{10}$$

$$\varphi(t) = \arctan(I(t)/Q(t)) + m\pi. \tag{11}$$

Here, $m\pi$ is used to unwrap the arctan function, where m is an integer number, so that the range of the demodulated phase changes from negative infinite to positive infinite [20]. In order to measure nanostrain quantitatively, it is necessary to confirm the quantitative relationship between strain and phase change. $\varphi(t)$ is the phase change resulting from the refraction index variation along the fiber, which can be expressed by $\varphi_i = 4\pi n z_i/\lambda$, where n is the refractive index of the fiber and z_i is the location along the fiber. The phase difference between two certain positions is given by

$$\varphi_{ij} = 4\pi n(z_j - z_i)/\lambda = 4\pi n z_{ij}/\lambda. \tag{12}$$

From Eq. (12), we can easily know that φ_{ij} would be a constant value if there are no external perturbations. When the strain is applied to the fiber, n and z_{ij} will change, which induces the change of φ_{ij}. By inducing the differential algorithm, we can get $\Delta\varphi_{ij} = \frac{4\pi}{\lambda}(n \cdot \Delta z_{ij} + \Delta n \cdot z_{ij})$, of which $\Delta z_{ij} = z_{ij} \cdot \Delta\epsilon$ and $\Delta n = C_\epsilon \cdot \Delta\epsilon$, where C_ϵ is the strain parameter of refractive index and $\Delta\epsilon$ represents the amount of strain applied to the fiber. We rewrite the equation as

$$\begin{aligned}\Delta\varphi_{ij} &= \frac{4\pi}{\lambda}(n \cdot z_{ij} \cdot \Delta\epsilon + C_\epsilon \cdot \Delta\epsilon \cdot z_{ij}) \\ &= \frac{4\pi}{\lambda}(n + C_\epsilon) \cdot z_{ij}\Delta\epsilon.\end{aligned} \tag{13}$$

According to Eq. (13), the phase difference $\Delta\varphi_{ij}$ is proportional to the strain $\Delta\epsilon$, so that the linear relationship between them makes it possible to measure strain quantitatively. The larger the interval, the greater the strain sensitivity of phase difference. However, the interval between z_i and z_j can actually limit the spatial resolution at the same time. To balance these two restrictions, the strain sensitivity of the system can be defined as

$$\frac{\Delta\varphi_{ij}}{z_{ij}\Delta\epsilon} = \frac{4\pi}{\lambda}(n + C_\epsilon). \tag{14}$$

Here, one thing that should be pointed out is that the refractive index of the fiber is about 1.46, while the strain parameter of refractive index C_ϵ differs from −0.16 to $-0.63\epsilon^{-1}$ for different kinds of fiber [22–24]. Therefore, the change of length of fiber due to strain plays a major role in the phase difference. Moreover, the strain parameter of the refractive index of the fiber we used can be calculated by Eq. (14).

3. EXPERIMENT AND RESULTS

The schematic diagram of the experimental setup is shown in Fig. 2. The laser source comes from a semiconductor laser with a narrow linewidth of 3 kHz. The output wavelength is

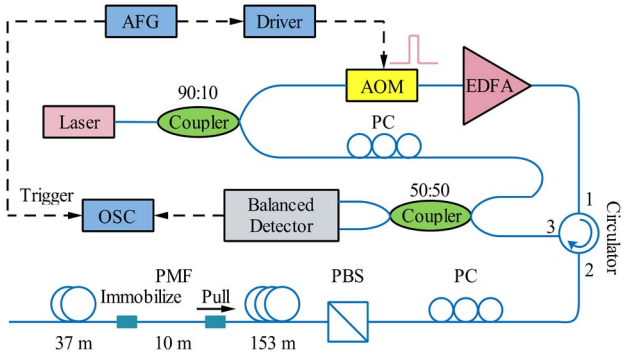

Fig. 2. Nano-strain sensing experimental setup. AFG, arbitrary function generator; AOM, acousto-optical modulator; PMF, polarization maintaining fiber; EDFA, erbium-doped fiber amplifier; PC, polarization controller; OSC, oscilloscope; PBS, polarization beamsplitter.

1550.06 nm, and the optical output power is 20 mW. The output of the laser is divided into two parts by a 90∶10 coupler, forming a signal and a local reference light. The signal light part is pulsed by an AOM with a pulse width of 20 ns and a repetition rate of 10 kHz. In addition, a frequency shift of 200 MHz to the signal light is introduced by the AOM. First, the signal pulse is amplified by an Er^{3+}-doped fiber amplifier (EDFA), and then it is injected into the sensing fiber with length of 200 m through a circulator. A nanopositioning translation stage (PI, P-620.1CD) with a resolution of 0.2 nm is employed to apply a variable and precise strain to the fiber. In single mode fiber, the polarization state of Rayleigh scattering light can be easily disturbed by external factors, so a Panda polarization maintaining fiber (PMF) is used here to maintain the polarization state and subsequently avoid the polarization fading. The polarization controller (PC) and the polarization beamsplitter (PBS) are used here to adjust the polarization to guarantee the Rayleigh scattering light only transmits in one axis of the PMF. Then the Rayleigh scattering light is combined with the local reference light. The AC component of the beat signal is detected by a balanced detector. The electrical signal is recorded by an oscilloscope with 5 GSa/s sampling rate. The phase of Rayleigh scattering light can be obtained by using I/Q demodulation, and the process of their demodulation is completed in a computer. Due to the high sensitivity to external vibration of Φ-OTDR, the experiment is conducted on the first floor at night to avoid the interference of the external environment.

Figure 3 shows the typical results of the demodulated amplitude and phase of the Rayleigh scattering light near the tensile region by using I/Q demodulation. From Fig. 3(a), the Rayleigh scattering traces show a jagged appearance, and the variation of the Rayleigh scattering traces start from 153 to 163 m, which conforms to the tensile region in our experiment. While out of the tensile region, the Rayleigh scattering traces overlap with each other completely. Subtracting the amplitude trace from the trace without stretching will show the amplitude variation at the tensile region more clearly, as illustrated in Fig. 3(c), so that the tensile region can be located precisely. Figure 3(b) shows the change of phase along the sensing fiber.

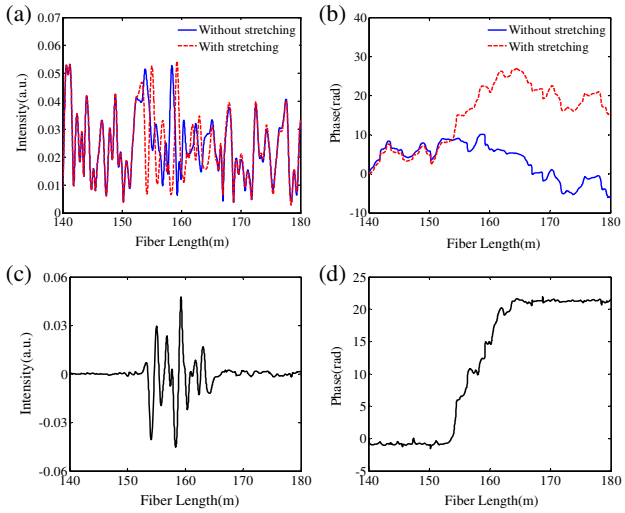

Fig. 3. (a) Amplitude and (b) phase of the Rayleigh scattering light near tensile region; the subtraction of (c) amplitude and (d) phase.

At the beginning of the sensing fiber, the phase traces overlap with each other, then they separate from each other from the start of tensile region, and the difference of phase increases linearly along with the sensing fiber until they are out of the tensile region, which is shown in Fig. 3(d). Consequently, the strain can be obtained by measuring the phase difference along with the sensing fiber. For phase demodulation, there are some issues that should be considered. The phase of the Rayleigh scattering trace accumulates increasingly along the fiber; so do the relative errors including demodulation errors, frequency instability, and phase noise of the laser. For instance, as is shown in Fig. 3(d), some vibration exists in the linearly increasing section of phase due to the demodulation errors. In our experiment, we try to eliminate these errors by subtracting the phases of two certain positions and the moving average. Intervals of 2.5 and 5 m are used in our experiment and compared with each other. The nanopositioning translation stage is employed to apply various strains to the fiber. One end of the tensile region is immobilized, and the other end is pulled by the nanopositioning translation stage controlled by computer. For stepping mode, the nanopositioning translation stage moves step by step. The step-hold time is 35 ms, and the amount of strain can be controlled. For example, if the step is set to 100 nm, the length of the tensile region in our experiment is 10 m, so that the strain step can be 10 nϵ.

Figure 4 shows the phase demodulation results of various strain steps in different intervals. By subtracting the phases of two certain positions and the moving average, the noise is suppressed very well, and the minimum fluctuation that can be distinguished is 0.045 rad in 5-m interval and 0.047 rad in 2.5-m intervals as shown in Fig. 4(a). A stair-stepping pattern is shown in the results due to the nanopositioning translation stage working in a step-by-step model. The relative altitude of the stairs represents the amount of phase difference induced by strain. With the increasing strain, the amount of phase difference increases as well. The rise time is 10 ms, which represents the response time of closed-loop control. Under the same strain, the amount of phase difference of the 2.5-m interval

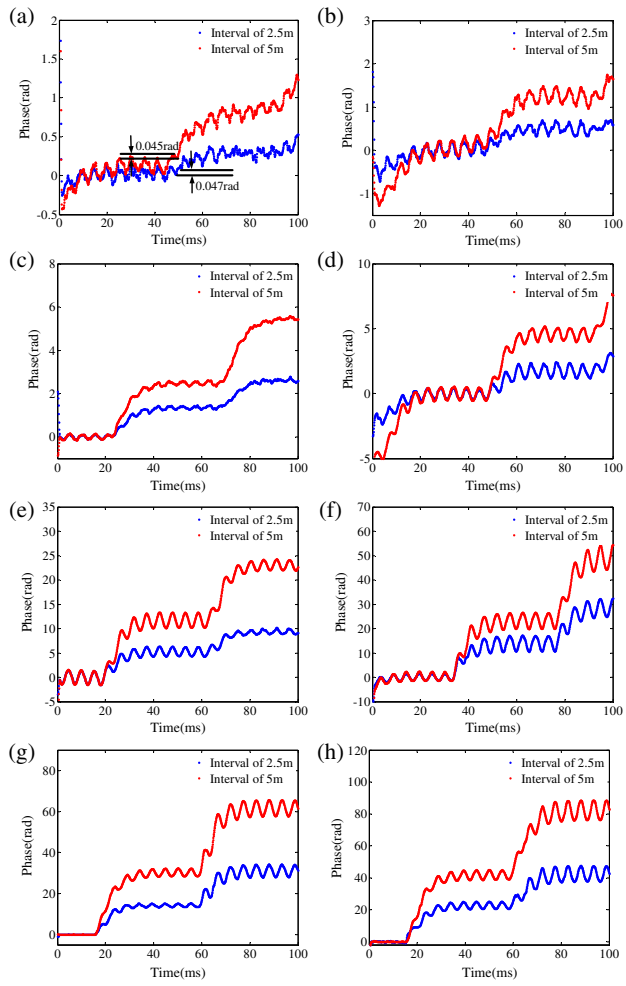

Fig. 4. Phase demodulation of various strain steps. (a) 10 nϵ, (b) 20 nϵ, (c) 50 nϵ, (d) 100 nϵ, (e) 250 nϵ, (f) 500 nϵ, (g) 750 nϵ, (h) 1000 nϵ.

is about half of the 5-m interval, which conforms to the theoretical analysis. The step-hold time is about 35 ms, corresponding to the step-hold time of the nanopositioning translation stage. Furthermore, it should be noted that a sine-wave oscillation exists on the stepped surface. That is because the fiber keeps vibrating after pulling the fiber, and the frequency of this vibration is equal to the resonant frequency of this tensile section. In addition, we can find that with the increasing of strain, the intensity of this vibration increases as well, which may induce more errors of measurement when measuring the relative altitude of stairs.

Based on the above phase demodulation of various strain steps, the phase difference with a strain range of 10–1000 nϵ is measured, which is shown in Fig. 5. The dots represent the measured data, while the red and green solid lines represent the fitting results with intervals of 5 and 2.5 m, respectively. The phase difference is linear to strain, the slope of the red fitting line is 0.04357 rad/nϵ, and R-square is 0.998 when the interval is 5 m, corresponding to 5 m spatial resolution. The spatial resolution can be up to 2.5 m, when the interval is 2.5 m, while the slope of the green fitting line is

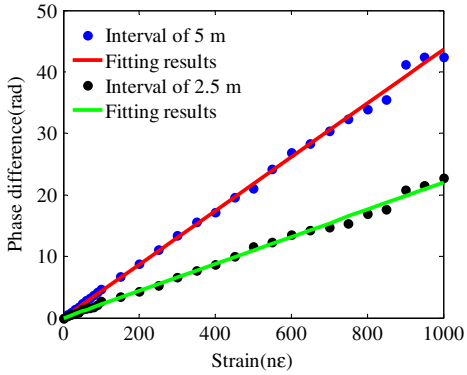

Fig. 5. Phase difference versus strain applied to a nanopositioning stage.

0.02202 rad/nϵ and R-square is 0.996. Thus it can be seen that the spatial resolution and strain sensitivity of phase difference restrict each other. In practice, we can choose the most appropriate interval to demodulate the phase according to different demands. Due to the better fitting result, the slope of the red fitting line is used to calculate the strain sensitivity of the system by Eq. (14), which can be calculated to be 8.714 mrad/(nϵ · m). The strain parameter of refractive index C_ϵ can also be calculated to be $-0.3751\epsilon^{-1}$. In addition, the linear fit is not so good when under large strain; that is because the vibration gives rise to measuring errors, and with the increasing strain, the intensity of this vibration increases as well, so that more measuring errors can be induced, which has been illustrated in Fig. 4. As is shown in Fig. 4(a), the sine-wave oscillation can be measured clearly, of which the minimum fluctuations that can be distinguished are 0.045 rad in 5-m intervals and 0.047 rad in 2.5-m intervals. According to the strain sensitivity of phase difference we have measured, the strain resolution of our system can reach to 1 nϵ at intervals of 5 m, and 2 nϵ at intervals of 2.5 m.

On the strength of the above quantitative relationship between phase difference and strain, the nanopositioning translation stage scanning with triangular wave is controlled to test the dynamic performance of our system. For scan mode, the nanopositioning translation stage moves continuously with a limited scan speed. For example, if the scan range of the stage is 0–1000 nm, the length of the tensile region is 10 m, so that the scan range of strain can be 0–100 nϵ. The cycle of the scan is 83 ms, so that the frequency is 12 Hz. The strain can be obtained in real time according to the quantitative relationship we have measured as shown in Fig. 6, of which the strain range is 0–100 nϵ and the frequency is 12 Hz. The jags in the strain trace are due to the vibration of fiber induced by the nanopositioning translation stage. In theory, the frequency response depends on the repetition rate of laser pulses in the experiment, which is 10 kHz. According to the Nyquist criteria, the maximum response frequency of the system is 5 kHz. However, limited to the scanning speed, the frequency of the triangular wave cannot be too high, so that it is not proper to evaluate the dynamic performance of the system by using the measured result in Fig. 6.

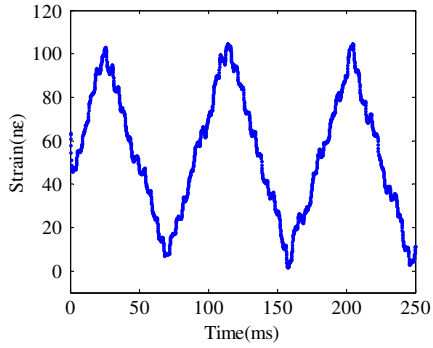

Fig. 6. Dynamic strain measured result with a range of 0–100 nϵ.

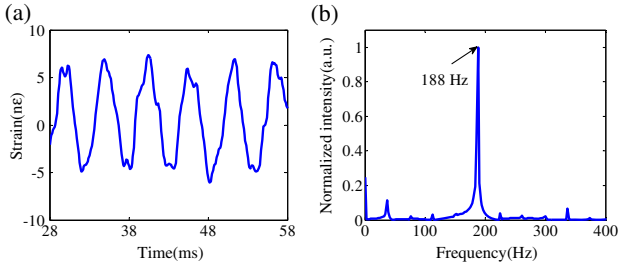

Fig. 7. Resonant signal of tensile section (a) in time domain and (b) in frequency domain.

According to the results in Fig. 4, our system can still respond to the vibration caused by stretch. The vibration section of Fig. 4(b) is taken out to further analyze, which is shown in Fig. 7. Figure 7(a) is the resonant signal in the time domain, where we can see that the resonant signal is in the form of a sine wave, and the range of strain is only from −5 to 5 nϵ. The frequency of the resonant signal reaches 188 Hz, which is shown in Fig. 7(b). It is proved that our system has the ability of responding to rapid nanostrain in real time. Due to the tiny nanostrain range (−5 to 5 nϵ) and some external noise introduced by frequency instability and phase noise of the laser, some frequency noise can exist in the measured results, as is shown in Fig. 7(b).

4. CONCLUSION

In summary, we present a nanostrain sensing system by introducing an efficient phase and amplitude demodulation scheme in Φ-OTDR. A nanopositioning translation stage is utilized to apply precise nanostrain to fiber. The quantitative relationship between phase variation and strain is theoretically analyzed and experimentally proved. A nanostrain sensing system with a large strain sensing range of 10–1000 nϵ and a strain resolution of 1 or 2 nϵ corresponding to a spatial resolution of 5 or 2.5 m, respectively, is demonstrated. The strain sensitivity of the system is measured to be 8.714 mrad/(nϵ · m), and the strain parameter of the refractive index of the sensing fiber is also measured to be $-0.3751\epsilon^{-1}$. The dynamic strain sensing is experimentally demonstrated; the measured frequency response of our system can reach 188 Hz. This sensing system has potential in quantitative measurements of large-range dynamic nanostrain.

Funding. National Key Technology Research and Development Program of the Ministry of Science and Technology of the People's Republic of China (MOST) (2014BAG05B07); National High Technology Research and Development Program of China 863 Program (2014AA110401); National Key Scientific Instrument and Equipment Development Project (2013YQ040815); National Natural Science Foundation of China (NSFC) (61308004, 61575052); Scientific Research Fund of Heilongjiang Provincial Education Department (12531093).

REFERENCES

1. Y. K. Dong, D. X. Ba, T. F. Jiang, D. W. Zhou, H. Y. Zhang, C. Y. Zhu, Z. W. Lu, H. Li, L. Chen, and X. Y. Bao, "High-spatial-resolution fast BOTDA for dynamic strain measurement based on differential double-pulse and second-order sideband of modulation," IEEE Photon. J. **5**, 2600407 (2013).
2. T. V. A. Tran, Y. G. Han, H. Y. J. Lee, S. H. Kim, and S. B. Lee, "Performance enhancement of long-distance simultaneous measurement of strain and temperature based on a fiber Raman laser with an etched FBG," IEEE Photon. Technol. Lett. **17**, 1920–1922 (2005).
3. J. M. Henault, J. Salin, G. Moreau, J. Bertand, F. Taillade, M. Quiertant, and K. Benzarti, "Monitoring of concrete structures using OFDR technique," AIP Conf. Proc. **1335**, 1386–1393 (2011).
4. Q. Liu, Z. He, and T. Tokunaga, "Sensing the earth crustal deformation with nano-strain resolution fiber-optic sensors," Opt. Express **23**, A428–A436 (2015).
5. H. F. Taylor and C. E. Lee, "Apparatus and method for fiber optic intrusion sensing," U.S. patent 5,194,847 (16 March 1993).
6. Z. Qin, T. Zhu, L. Chen, and X. Bao, "High sensitivity distributed vibration sensor based on polarization-maintaining configurations of phase-OTDR," IEEE Photon. Technol. Lett. **23**, 1091–1093 (2011).
7. T. Zhu, Q. He, X. H. Xiao, and X. Y. Bao, "Modulated pulses based distributed vibration sensing with high frequency response and spatial resolution," Opt. Express **21**, 2953–2963 (2013).
8. T. Zhu, X. H. Xiao, Q. He, and D. M. Diao, "Enhancement of SNR and spatial resolution in Φ-OTDR system by using two-dimensional edge detection method," J. Lightwave Technol. **31**, 2851–2856 (2013).
9. Z. N. Wang, J. J. Zeng, J. Li, M. Q. Fan, H. Wu, F. Peng, L. Zhang, Y. Zhou, and Y. J. Rao, "Ultra-long phase-sensitive OTDR with hybrid distributed amplification," Opt. Lett. **39**, 5866–5869 (2014).
10. L. Zhou, F. Wang, X. C. Wang, Y. Pan, Z. Q. Sun, J. Hua, and X. P. Zhang, "Distributed strain and vibration sensing system based on phase-sensitive OTDR," IEEE Photon. Technol. Lett. **27**, 1884–1887 (2015).
11. S. Wang, X. Y. Fan, Q. W. Liu, and Z. Y. He, "Distributed fiber-optic vibration sensing based on phase extraction from time-gated digital OFDR," Opt. Express **23**, 33301–33309 (2015).
12. X. Tu, Q. Sun, W. Chen, M. Chen, and Z. Meng, "Vector Brillouin optical time-domain analysis with heterodyne detection and IQ demodulation algorithm," IEEE Photon. J. **6**, 1–8 (2014).
13. Y. Koyamada, Y. Eda, S. Hirose, S. Nakamura, and K. Hogari, "Novel fiber-optic distributed strain and temperature sensor with very high resolution," IEICE Trans. Commun. **89**-B, 1722–1725 (2006).
14. Y. Koyamada, M. Imahama, K. Kubota, and K. Hogari, "Fiber-optic distributed strain and temperature sensing with very high measurand resolution over long range using coherent OTDR," J. Lightwave Technol. **27**, 1142–1146 (2009).
15. A. Masoudi, M. Belal, and T. P. Newson, "A distributed optical fibre dynamic strain sensor based on phase-OTDR," Meas. Sci. Technol. **24**, 085204 (2013).
16. C. Wang, C. Wang, Y. Shang, X. Liu, and G. Peng, "Distributed acoustic mapping based on interferometry of phase optical time-domain reflectometry," Opt. Commun. **346**, 172–177 (2015).
17. G. S. Fang, T. W. Xu, S. W. Feng, and F. Li, "Phase-sensitive optical time domain reflectometer based on phase-generated carrier algorithm," J. Lightwave Technol. **33**, 2811–2816 (2015).
18. Z. Pan, K. Liang, Q. Ye, H. Cai, R. Qu, and Z. Fang, "Phase-sensitive OTDR system based on digital coherent detection," Proc. SPIE **8311**, 83110S (2011).
19. Z. Wang, L. Zhang, S. Wang, N. Xue, F. Peng, M. Fan, W. Sun, X. Qian, J. Rao, and Y. Rao, "Coherent Φ-OTDR based on *I*/*Q* demodulation and homodyne detection," Opt. Express **24**, 853–858 (2016).
20. G. Tu, X. Zhang, Y. Zhang, and F. Zhu, "The development of an OTDR system for quantitative vibration measurement," IEEE Photon. Technol. Lett. **27**, 1349–1352 (2015).
21. Y. L. Lu, T. Zhu, L. A. Chen, and X. Y. Bao, "Distributed vibration sensor based on coherent detection of phase-OTDR," J. Lightwave Technol. **28**, 3243–3249 (2010).
22. A. H. Hartog, A. J. Conduit, and D. N. Payne, "Variation of pulse delay with stress and temperature in jacketed and unjacketed optical fibres," Opt. Quantum Electron. **11**, 265–273 (1979).
23. J. J. Carr, S. L. Saikkonen, and D. H. Williams, "Refractive-index measurements on single-mode fiber as functions of product parameters, tensile-stress, and temperature," Fiber Integr. Opt. **9**, 393–396 (1990).
24. L. B. Yuan, "Effect of temperature and strain on fiber optic refractive index," Acta Opt. Sin. **17**, 1713–1717(1997).